



**HAL**  
open science

## Etching of GeSe<sub>2</sub> chalcogenide glass and its pulsed laser deposited thin films in SF<sub>6</sub>, SF<sub>6</sub>/Ar and SF<sub>6</sub>/O<sub>2</sub> plasmas

T Meyer, G Ledain, A Girard, A Rhallabi, M Bouška, P Němec, Virginie Nazabal, C Cardinaud

### ► To cite this version:

T Meyer, G Ledain, A Girard, A Rhallabi, M Bouška, et al.. Etching of GeSe<sub>2</sub> chalcogenide glass and its pulsed laser deposited thin films in SF<sub>6</sub>, SF<sub>6</sub>/Ar and SF<sub>6</sub>/O<sub>2</sub> plasmas. Plasma Sources Science and Technology, 2020, 29 (10), pp.105006. 10.1088/1361-6595/abb0d0 . hal-03011508

**HAL Id: hal-03011508**

**<https://hal.science/hal-03011508>**

Submitted on 25 Nov 2020

**HAL** is a multi-disciplinary open access archive for the deposit and dissemination of scientific research documents, whether they are published or not. The documents may come from teaching and research institutions in France or abroad, or from public or private research centers.

L'archive ouverte pluridisciplinaire **HAL**, est destinée au dépôt et à la diffusion de documents scientifiques de niveau recherche, publiés ou non, émanant des établissements d'enseignement et de recherche français ou étrangers, des laboratoires publics ou privés.

# Etching of GeSe<sub>2</sub> chalcogenide glass and its pulsed laser deposited thin films in SF<sub>6</sub>, SF<sub>6</sub>/Ar and SF<sub>6</sub>/O<sub>2</sub> plasmas

T. Meyer<sup>1</sup>, G. Le Dain<sup>1</sup>, A. Girard<sup>1</sup>, A. Rhallabi<sup>1</sup>, M. Bouška<sup>2</sup>,  
P. Němec<sup>2</sup>, V. Nazabal<sup>3</sup>, C. Cardinaud<sup>1</sup>

<sup>1</sup> Université de Nantes, CNRS, Institut des Matériaux Jean Rouxel, IMN, F-44000 Nantes, France

<sup>2</sup> Department of Graphic Arts and Photophysics, Faculty of Chemical Technology, University of Pardubice, Studentská 573, 53210 Pardubice, Czech Republic

<sup>3</sup> Univ Rennes, CNRS, ISCR (Institut des Sciences Chimiques de Rennes) – UMR 6226, F-35000 Rennes, France

## Abstract.

Excited species, reactive neutral species and positive ions, produced during the etching of Ge, Se and GeSe<sub>2</sub> targets in Inductively Coupled Plasmas, were identified by means of Mass Spectrometry (MS) and Optical Emission Spectroscopy (OES). The surface of etched Ge<sub>39</sub>Se<sub>61</sub> thin films were analysed thanks to *in situ* X-ray photoelectron spectroscopy (XPS) and compared with those of Ge and Se etched samples. In 100% SF<sub>6</sub>, the successive adsorption of fluorine atoms forms SeF<sub>*x*</sub> (*x* = 2, 4, 6) and GeF<sub>*x*</sub> (*x* = 2, 4) stable and volatile products, generating a surface with few residues as interpreted with *in situ* XPS. The identification of SSeF<sub>*x*</sub><sup>+</sup> (*x* = 2, 3, 7) ions confirms that sulfur atoms play a role during the etching of Se-containing materials. A 0D kinetic model predicted the evolution of reactive neutral fluxes, ion fluxes and plasma parameters (*T<sub>e</sub>* and *n<sub>e</sub>*) in SF<sub>6</sub>/Ar plasmas. It was found that the SeF<sub>6</sub> and GeF<sub>4</sub> concentrations, through SeF<sub>5</sub><sup>+</sup> and GeF<sub>3</sub><sup>+</sup> MS signals, were related to the fluorine atom flux. In SF<sub>6</sub>/O<sub>2</sub>, the simultaneous effect of fluorine and oxygen adsorption induces (Se)<sub>*x*</sub>-Ge-R<sub>4-*x*</sub> environments (R = F, O) at the surface of the Ge<sub>39</sub>Se<sub>61</sub> thin films.

*Keywords:* GeSe<sub>2</sub>, chalcogenide, thin film, etching, SF<sub>6</sub>

Submitted to: *Plasma Sources Sci. Technol.*

## 1 Introduction

Amorphous thin films and chalcogenide glasses have drawn increasing attention due to their optical properties as a wide transparency window (up to 16 μm for selenides), a high nonlinear refractive index [1, 2], low phonon energy [3, 4], photosensitivity [5, 6]. Hence they are adapted for photonic applications [7, 8]. Aiming for low-cost and miniaturized devices, deposition and patterning techniques make possible fabrications of integrated multiple components onto the same substrate, contributing to the development of complex integrated optical platforms. Most of deposition processes are based on physical vapor deposition method as thermal evaporation [9, 10], sputtering [11, 12], Pulsed

Laser Deposition (PLD) [13,14]. As patterning method, plasma etching can provide an anisotropic sidewall profile on dielectric materials with low sidewall roughness. In recent years, some chalcogenides as As-S [15], Ge-Sb-Te [16], Ge-Sb-Se [17], Ge-Sb-S [18], Ge-As-Se [19], Ga-Ge-Sb-S [20] or Ga-Ge-Sb-Se [21] were patterned using mostly fluorine-based plasmas (CHF<sub>3</sub> and CF<sub>4</sub>).

Among the Ge-Se system, bulk glasses and thin films have been characterized according to its composition by nuclear magnetic resonance and Raman spectroscopies, neutron/electron/x-ray diffraction and density-functional based molecular dynamics simulations [22–28]. In the case of the stoichiometric GeSe<sub>2</sub>, structural analysis proposed the [GeSe<sub>4/2</sub>] tetrahedra (Td) as the dominant structural motif, which can be linked by corners (corner-shared (CS) tetrahedra) or edges (edge-shared (ES) tetrahedra). In addition, the presence of Ge-Ge and Se-Se homopolar bonds (allowed by relatively close electronegativities of Ge (2.01) and Se (2.55) atoms) is expected and probably over- or under-coordinated atoms as well. The proportion of [GeSe<sub>4/2</sub>] Td CS and ES motifs, homopolar bonds and coordination defects evolves according to the composition of the Ge<sub>x</sub>Se<sub>100-x</sub> glasses. The occurrence of above-mentioned structural units is also observed within ternary systems as Ge-Sb-Se [29], Ge-As-Se [30,31] or Ga-Ge-Se [32,33]. Their respective proportions in the amorphous thin films and glass materials depend on their chemical compositions, their thermal history and/or method of manufacture. Nevertheless, there is no pertinent study about the etching of Ge-Se glasses and corresponding thin films.

During an etching process, radical species (*e.g.* F, Cl, Br in halogen plasmas) are lost by recombination in the plasma volume or onto the sample surface and the reactor wall by pumping or by adsorption on a material. Subsequently, the process leads to the formation of volatile products at the sample surface and desorption from the surface leads to the formation of new products by recombination into the plasma. Fluorine-based chemistries (SF<sub>6</sub>, CF<sub>4</sub>, *etc.*) are extensively used for Ge etching due to the volatility of the GeF<sub>4</sub> etch product. Etching characteristics of Ge have been investigated and often compared with those of Si [34–37]. With a growing interest for patterned Ge structures, many works have been carried out to understand the influence of the etching conditions on the Ge surface [38–41]. Furthermore, the monitoring of germanium-fluorinated species established the relation between the etch rate and the concentration of etch products [34,35]. To the best of our knowledge, the etching of pure selenium was not investigated. Although a selenium-based material as ZnSe is etched in methane-based plasmas [42–44], there is a lack of information about the etch products as well as fluorine-selenium interactions.

In this paper, the etching of Ge<sub>39</sub>Se<sub>61</sub> thin films and a GeSe<sub>2</sub> glass target is investigated using SF<sub>6</sub>, SF<sub>6</sub>/Ar and SF<sub>6</sub>/O<sub>2</sub> plasmas. The coupling of Mass Spectrometry (MS) and Optical Emission Spectroscopy (OES) reveals some fundamental properties of the Se<sub>x</sub>S<sub>y</sub>F<sub>z</sub> species and point out reactional kinetic of fluorinated Ge and Se. Along with plasma characterization, plasma modeling offers a better understanding of the plasma/surface interaction. Besides, *in situ* X-ray Photoelectron Spectroscopy

(XPS) is performed to identify nonvolatile products (GeO<sub>2</sub>, GeO<sub>4</sub> and GeSe<sub>x</sub>O<sub>y</sub>F<sub>z</sub> species) at the surface as well as species with unsaturated covalent bonds (GeF and GeO species).

## 2 Method

Ge-Se thin films, with a thickness of 1  $\mu\text{m}$ , were deposited by PLD, via ablating a GeSe<sub>2</sub> bulk target with an excimer laser (COMPex 205, Coherent) operating at 248 nm. The details of glass target fabrication and PLD process are given elsewhere [14]. In a previous study, the composition of Ge<sub>39</sub>Se<sub>61</sub> thin films was determined using a scanning electron microscope with an energy-dispersive X-ray analyzer (EDS, JSM 6400-OXFORD Link INCA). In the present study, the same atomic proportions were found using X-Ray Photoelectron Spectroscopy (Kratos Axis NOVA). Nevertheless, it should be emphasized that XPS analysis describes the surface composition. A GeSe<sub>2</sub> glass target ( $r = 2.5$  cm) as well as vitreous selenium (4N pellets; Codex International) and germanium (5N 4" wafer; Goodfellow) were etched for comparison.

Etching was performed using an Inductively Coupled Plasma reactor operating at 13.56 MHz. Configuration of the plasma source and dimension of the diffusion chamber are similar to that of an Alcatel 601E. For the SF<sub>6</sub>/Ar and SF<sub>6</sub>/O<sub>2</sub> mixtures, the total flow rate was varied to conserve a fixed total pressure when varying the feed gas composition. The substrate holder consisted in a 100 mm in diameter stainless steel plate mechanically clamped to the bottom electrode. This electrode was unbiased, thus ions struck the sample with a mean kinetic energy close to the plasma potential ( $< 10$  eV). Substrate holder temperature was maintained at 20°C thanks to He backside cooling.

Optical Emission Spectroscopy (OES) was performed using a Horiba iHR550 monochromator. The detection was provided by a CCD camera (SYNAPSE). Two shutters, one after the aperture and one before the camera, set the exposure time. Both slit aperture and exposure time were set to prevent the saturation of the signal. Excited states were monitored using the emission lines reported in table 1. Argon gas was used as an actinometer in the SF<sub>6</sub>/O<sub>2</sub> plasma with a partial pressure fixed at 0.2 mTorr (2% of the total pressure). In that way, we have information about the variation of the atomic fluorine and the atomic oxygen densities as a function of the O<sub>2</sub> percentage. However, actinometry is not valid in SF<sub>6</sub>/Ar plasma since the argon addition changes the electron energy distribution [45,46]; and also for the Ge and Se emission lines, since their energy threshold is far below those of the Ar emission lines. Besides, there are no consistent studies about the excitation cross-sections by electronic impact of Ge and Se excited states.

A mass analyzer (Hiden Analytical EQP 1000) was used for studying the plasma chemistry. The pumping system maintained the pressure inside the spectrometer below  $1 \times 10^{-7}$  Torr. Particles enter the mass spectrometer via a 100  $\mu\text{m}$  diameter orifice. At the entrance of the mass spectrometer, a potential may be applied on a

Table 1: Spectroscopic data for Ge, Se, F, Ar and O atoms [47].

Atom	Energy threshold (eV)	Transition	Wavelength (nm)
Ge	4.85	4p5s <sup>3</sup> P <sub>2</sub> <sup>0</sup> → 4p <sup>2</sup> <sup>3</sup> P <sub>2</sub>	265.1
Se	8.59	4p <sup>3</sup> 6p <sup>5</sup> P → 4p <sup>3</sup> 5s <sup>3</sup> S <sup>0</sup>	473.0
F	14.75	3p <sup>2</sup> P <sub>3/2</sub> <sup>0</sup> → 3s <sup>2</sup> P <sub>5/2</sub> <sup>0</sup>	703.7
Ar	13.48	3p <sup>5</sup> (2P <sub>1/2</sub> <sup>0</sup> ) 4p → 3p <sup>5</sup> (2P <sub>1/2</sub> <sup>0</sup> ) 4s	750.4
O	10.99	2s <sup>2</sup> 2p <sup>3</sup> (4S <sup>0</sup> ) 3p → 2s <sup>2</sup> 2p <sup>3</sup> (4S <sup>0</sup> ) 3s	844.6
Ar	13.08	3p <sup>5</sup> (2P <sub>3/2</sub> <sup>0</sup> ) 4p → 3p <sup>5</sup> (2P <sub>3/2</sub> <sup>0</sup> ) 4s	811.5

first lens in order to repulse or to attract plasma ions. For the analysis of reactive neutrals, this potential was set so that nothing but positive ions, which were formed in the spectrometer ionisation source, were detected. The appearance potentials were determined by sweeping the electron energy from 1 to 50 eV.

The chemical bonding characteristics of Ge, Se and Ge<sub>39</sub>Se<sub>61</sub> samples were examined by *in situ* X-ray Photoelectron Spectroscopy. The equipment consists of a monochromatic Al K $\alpha$  X-ray source (SPECS XR 50 M and FOCUS 500) at 1486.6 eV and a hemispherical analyzer (SPECS Phoibos 150 HR). The analysis chamber was connected to the etching chamber through an ultra-high vacuum chamber, in order to limit surface contamination. The operating pressure in the analysis chamber was  $1 \times 10^{-9}$  mbar. Spectra were recorded with a pass energy of 14 eV, with an energy step of 0.1 eV. Samples were neutralized with an electron flood gun to compensate for the charging effect shift. Data processing of Ge 2p<sub>3/2</sub>, Se 3p, Se 3d and Ge 3d spectra was done by the CASA-XPS software using a Shirley background [48] and a Lorentzian function convoluted with a Gaussian. Each doublet was constrained with an identical Full Width at Half Maximum (FWHM). Energy calibration of Ge, Se and Ge<sub>39</sub>Se<sub>61</sub> samples was performed using the Ge-Ge bond (binding energy, BE = 29.0 eV), Se-Se bond (BE = 55.3 eV) and the (Ge)-Se-Ge environment (BE = 54.7 eV). The latter were retrieved from *ex situ* XPS analysis (Kratos Axis NOVA) of as received Ge, Se and Ge<sub>39</sub>Se<sub>61</sub> samples and using the C-C bond (BE = 284.8 eV).

We used a kinetic model developed previously for RF (13.56 MHz) ICP in SF<sub>6</sub>/Ar mixture [49–51]. Using consistent cross-section data [52–57], the rate coefficients are integrated over a Maxwellian electron energy distribution. The model is based on the solving of mass-balance equations where rate coefficients are injected, setting the gain and loss rates of different species. This set of equations is coupled to the neutrality equation and power balance equation to determine the electronic density ( $n_e$ ) and the electronic temperature ( $T_e$ ), respectively. In the present study, we used this model to provide detailed kinetic information about reactive neutrals and charged species (electrons and positive ions) when operating in SF<sub>6</sub>/Ar plasma. In order to illustrate the excitation and ionization reaction probabilities, the different electronic temperatures were used as input parameters to calculate Maxwell-Boltzmann distributions.

### 3 Results and discussion

Figure 1 shows the vapor pressure data and the boiling temperature of some fluorinated compounds. Chemical etching relies on the desorption of etch products. Nevertheless, the mechanism is highly dependent on the pressure/temperature values. In the best-case scenario, the vapor pressures can be retrieved from Antoine coefficients as for SeF<sub>4</sub> and SeF<sub>6</sub> molecules [58]. For these species, the vapor pressure data are extrapolated for low-pressure processes. For a working pressure less than 20 mTorr, it is clear that GeF<sub>4</sub> and SeF<sub>6</sub> products are volatile at 20°C. Moreover, the vapor pressure of the SeF<sub>4</sub> and the boiling temperature of GeF<sub>2</sub> lead to predict that these molecules are volatile as well.

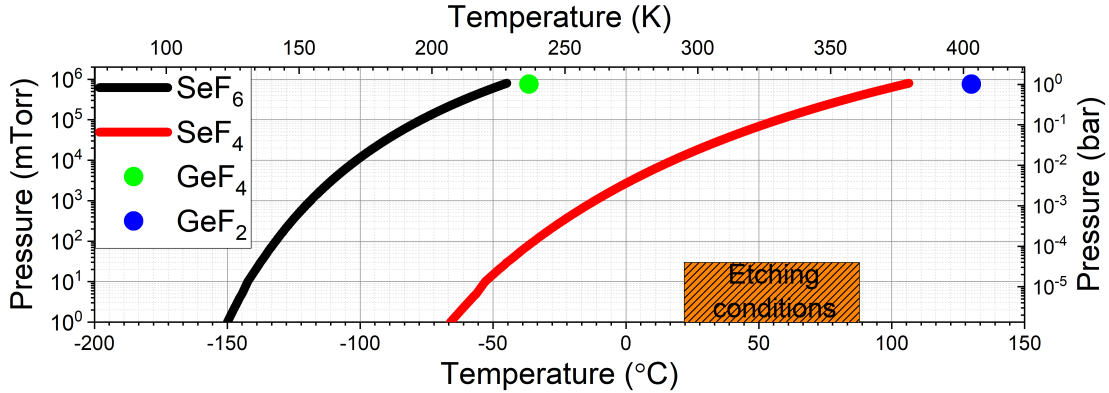


Figure 1: Extrapolated vapor pressures and boiling temperature of fluorinated products [58].

#### 3.1 Etch products in SF<sub>6</sub> plasma

**3.1.1 Reactive neutral species** In this section, all mentioned ions are produced inside the mass spectrometer source. Therefore, they are directly related to the plasma reactive neutrals products. An example is shown in figure 2 where GeF<sub>x</sub> and SeF<sub>x</sub> fragments are detected during the etching of the GeSe<sub>2</sub> glass target at 10 mTorr, 700 W, 20 sccm and without bias.

Unfortunately, literature about the dissociation and ionization of the SeF<sub>x</sub> ( $x = 1-6$ ) species is non-existent. We admit that SeF<sub>6</sub> is dissociated in SeF<sub>x</sub><sup>+</sup> ( $x = 1-5$ ) fragments similarly to SF<sub>6</sub> by direct ionization (1a) and dissociative ionization (1b) [56].

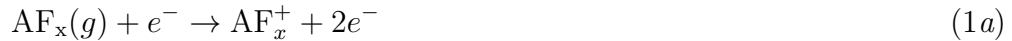


Table 2 lists the <sup>74</sup>GeF<sub>x</sub><sup>+</sup> and <sup>80</sup>SeF<sub>x</sub><sup>+</sup> products, their relative intensities and their appearance potentials. Relative intensities are calculated according to the GeF<sub>3</sub><sup>+</sup> and SeF<sub>5</sub><sup>+</sup> ions for the GeF<sub>x</sub><sup>+</sup> and SeF<sub>x</sub><sup>+</sup> ion clusters, respectively. Regarding relative

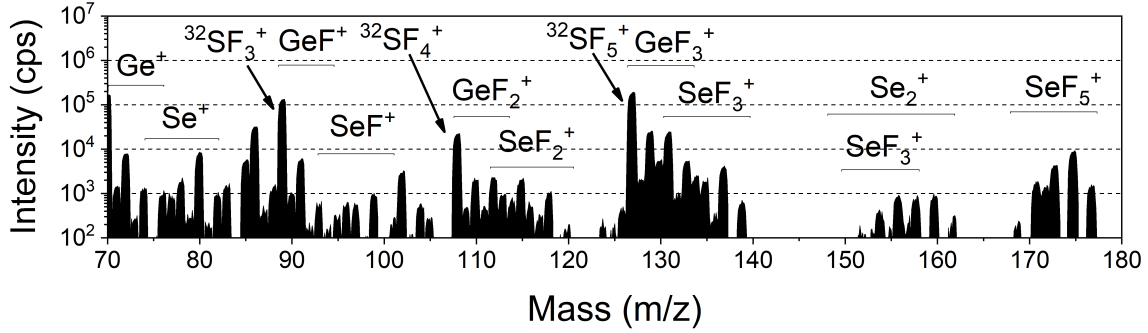


Figure 2: Mass spectrum recorded, at an electron energy of 70 eV, during the etching of the GeSe<sub>2</sub> glass target at 10 mTorr, 700 W, 20 sccm, without bias.

intensities of SeF<sub>x</sub><sup>+</sup> fragments, the dissociation of SeF<sub>x</sub> fragments shows a very similar fragmentation pattern to that of the SF<sub>6</sub> molecule [59].

Table 2: List of etch products which are observable during mass spectrometry analysis during the etching of the GeSe<sub>2</sub> glass target at 10 mTorr, 700 W, 20 sccm and without bias. *The margin of error for the appearance potential is ±1 eV.*

Ion	Mass (m/z)	Relative Intensity	Appearance potential (eV)
<sup>74</sup> GeF <sup>+</sup>	93	2.4	14.3
<sup>74</sup> GeF <sub>2</sub> <sup>+</sup>	112	9.3	12.3
<sup>74</sup> GeF <sub>3</sub> <sup>+</sup>	131	100	13.6
<sup>80</sup> SeF <sup>+</sup>	99	11.0	17.8
<sup>80</sup> SeF <sub>2</sub> <sup>+</sup>	118	11.2	13.6
<sup>80</sup> SeF <sub>3</sub> <sup>+</sup>	137	45.4	15.9
<sup>80</sup> SeF <sub>4</sub> <sup>+</sup>	156	9.9	13.0
<sup>80</sup> SeF <sub>5</sub> <sup>+</sup>	175	100	19.2

The direct ionization processes can be distinguished from the dissociative ionization processes since the former requires less energy for stable products to form ions. SeF<sub>5</sub><sup>+</sup> appearance potential (19.2 eV) clearly corresponds to the dissociative ionization of SeF<sub>6</sub>. Moreover, the appearance potentials of SeF<sub>2</sub><sup>+</sup> and SeF<sub>4</sub><sup>+</sup> are attributed to the direct ionization of SeF<sub>2</sub> and SeF<sub>4</sub> molecules, because both potentials are lower than those of SeF<sup>+</sup> and SeF<sub>3</sub><sup>+</sup>, respectively. In other words, SeF<sub>x</sub> ( $x = 2, 4, 6$ ) molecules enter in the spectrometer as stable products.

Following the same reasoning, GeF<sub>3</sub><sup>+</sup> appearance potential (13.6 eV) corresponds to the dissociative ionization processes of GeF<sub>4</sub>. Then, GeF<sub>2</sub><sup>+</sup> appearance potential (12.3 eV) corresponds to direct ionization of the GeF<sub>2</sub> molecule. For the latter, an ionization threshold energy was reported at 20.7 eV, during the fragmentation of the stable GeF<sub>4</sub>

molecule by electronic impact at 70 eV [60]. Our lower threshold energy confirms that the GeF<sub>2</sub> molecule enters inside the spectrometer source as a stable and volatile product. Therefore, GeF<sub>x</sub> ( $x = 2, 4$ ) are formed inside the etching chamber.

*3.1.2 Ionic species* As shown in figure 3, the plasma positive ions, coming from the etching chamber, can be identified.

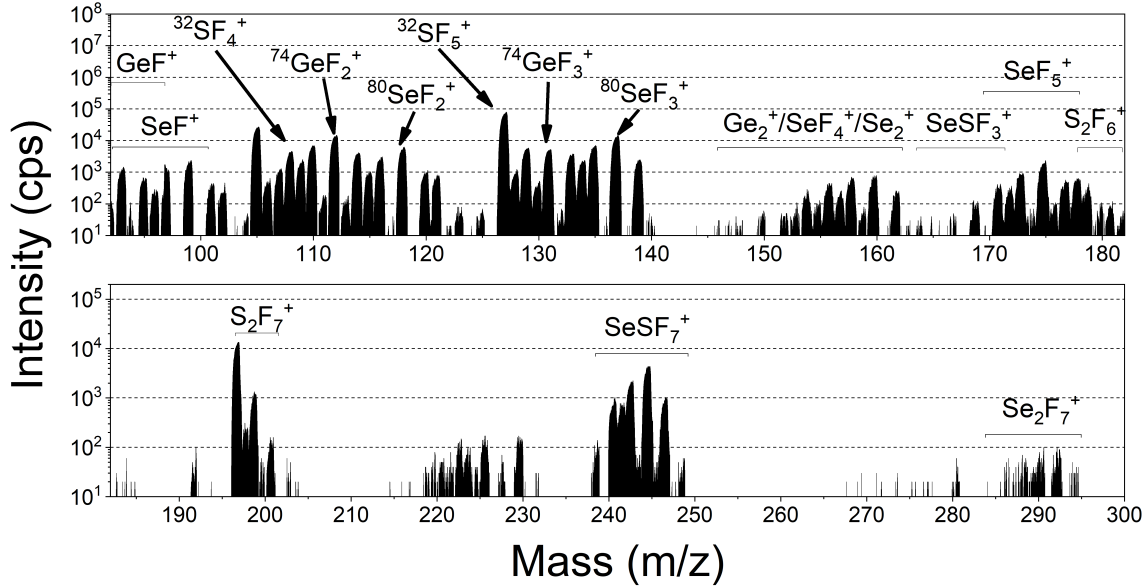
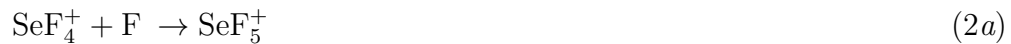


Figure 3: Ion mass spectra during the etching of GeSe<sub>2</sub> glass target at 20 mTorr, 700 W, 20 sccm and without bias.

SeF<sub>3</sub><sup>+</sup> and GeF<sub>2</sub><sup>+</sup> are the dominant ions among the SeF<sub>x</sub><sup>+</sup> and GeF<sub>x</sub><sup>+</sup> ionic products, respectively. SF<sub>3</sub><sup>+</sup> ( $m/z$  89) is not recorded to avoid the saturation of the MS detector. However, it is the most intense ion, regardless of the conditions, even if its total ionization cross-section is lower than that of the SF<sub>5</sub><sup>+</sup> ion [56]. These findings are in good agreement with those reported in a SF<sub>6</sub> discharge and was justified by the fact that the relative ion densities differ from relative ion intensities [61]. It has been demonstrated that ion-molecule reactions explain such results. By extension, ion-molecule reactions should not be exclusively restricted to SF<sub>x</sub><sup>+</sup> ions and may involve SeF<sub>x</sub><sup>+</sup> and GeF<sub>x</sub><sup>+</sup> ions (2a and 2b).



The presence of SeSF<sub>x</sub><sup>+</sup> ions is evidenced in figure 4 using SeS theoretical abundance pattern which is calculated using the isotopic abundances of Se and S atoms [62]. For the interpretation, the <sup>76</sup>SeF<sub>x</sub><sup>+</sup>, <sup>77</sup>SeF<sub>x</sub><sup>+</sup> and <sup>78</sup>SeF<sub>x</sub><sup>+</sup> intensities were subtracted using <sup>80</sup>SeF<sub>x</sub><sup>+</sup> ( $x = 4, 5$ ) intensities. From  $m/z$  144 to 152, a good agreement is found between

SeSF<sub>2</sub><sup>+</sup> theoretical pattern and experimental data ( $r_1 = 0.85$ ). Nevertheless, a higher correlation coefficient ( $r_2 = 0.94$ ) is obtained by addition of a Ge<sub>2</sub><sup>+</sup> theoretical abundance pattern to that of SeSF<sub>2</sub><sup>+</sup>. It is likely that the etching of the GeSe<sub>2</sub> glass target forms the Ge<sub>2</sub><sup>+</sup> ion from m/z 140 to 152. We report a second SeS pattern-like between m/z 163 and 171 which is attributed to SeSF<sub>3</sub><sup>+</sup>. Along with the <sup>82</sup>Se<sub>2</sub><sup>+</sup> ion (m/z 164), the signals at m/z 163 and 170 confirm the existence of more than two of ionic species within that mass range.

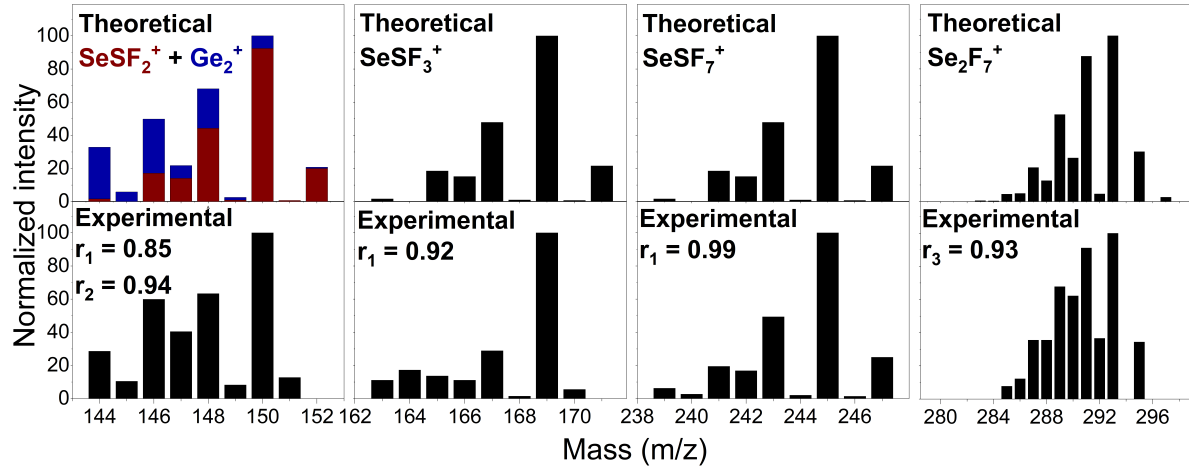
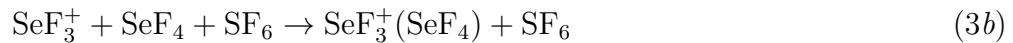


Figure 4: Comparison between theoretical abundance patterns and the mass spectrometry data during the etching of GeSe<sub>2</sub> glass target at 20 mTorr, 700 W, 20 sccm and without bias. Correlation coefficients  $r_1$ ,  $r_2$  and  $r_3$  are calculated using the SeS, SeS + Ge<sub>2</sub> and Se<sub>2</sub> theoretical abundance patterns, respectively.

No signal is detected in the mass range of the SeSF<sub>4</sub><sup>+</sup> (m/z 182 to 190) and SeSF<sub>5</sub><sup>+</sup> (m/z 201 to 209) theoretical patterns. One contribution (m/z 220 to 230) is not clearly identified. We suspect that there are more than one Se atom containing species. From m/z 239 to 247, the third SeS pattern-like is assigned to the SeSF<sub>7</sub><sup>+</sup> ion. An excellent match is found between the theoretical pattern and the MS data ( $r_1 = 0.99$ ) confirming the absence of other ions. A Se<sub>2</sub> pattern-like is assigned to the Se<sub>2</sub>F<sub>7</sub><sup>+</sup> ion from m/z 282 to 295. By analogy with the formation of S<sub>2</sub>F<sub>x</sub><sup>+</sup> ions [61, 63], we expect that SeSF<sub>7</sub><sup>+</sup> and Se<sub>2</sub>F<sub>7</sub><sup>+</sup> ions are formed by ion-molecule reactions between SeF<sub>x</sub> and/or SF<sub>x</sub> species (3a and 3b).



The identification of SeSF<sub>x</sub><sup>+</sup> ions is a strong evidence of ion-molecule reactions between SeF<sub>x</sub> species and the precursor fragments. The production of these ions implies a sulfur consumption.

**3.1.3 Nonvolatile species** Figure 5 presents the Ge 2p<sub>3/2</sub>, Se 3d and Ge 3d core levels after etching of the Ge and Se samples; and before (untreated sample) and after etching of the Ge<sub>39</sub>Se<sub>61</sub> thin film. Table 3 and table 4 list the fit values as the Binding Energy (BE), the Full Width at Half Maximum (FWHM), the spin-orbit splitting ( $\Delta E$ ) and the relative area extracted from the spectra in figure 5.

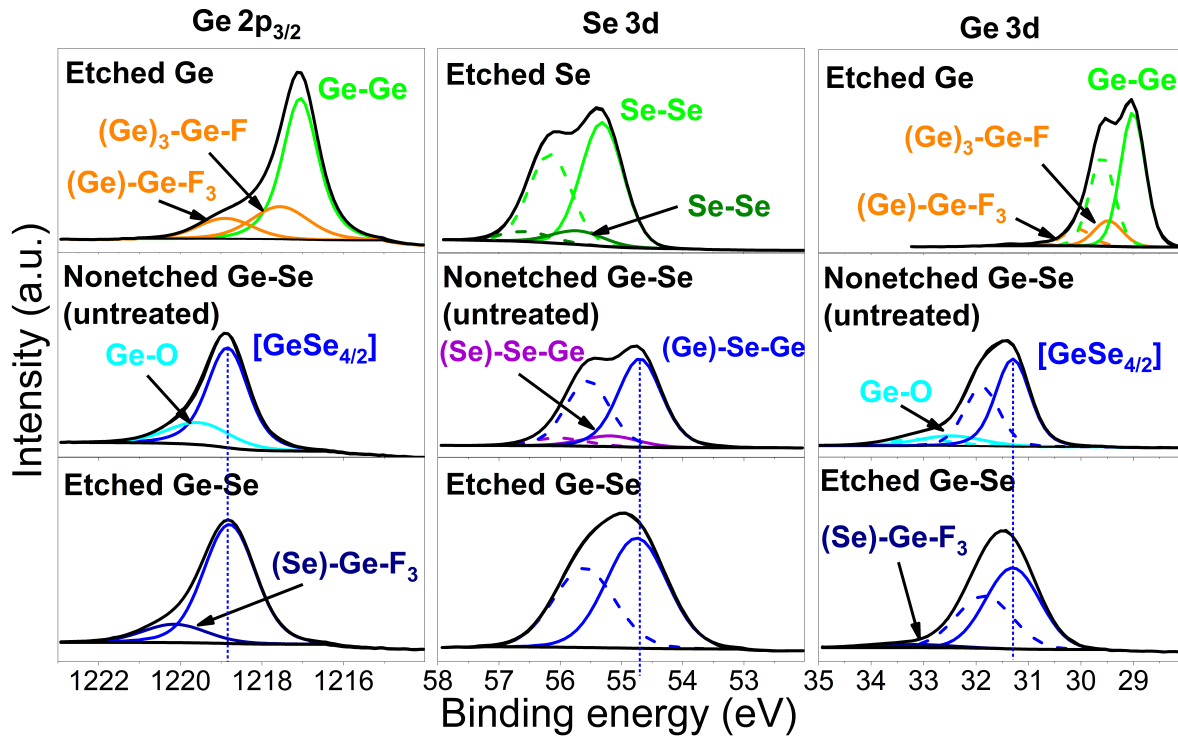


Figure 5: Ge 2p<sub>3/2</sub>, Se 3d and Ge 3d XPS spectra after the etching of Ge and Se samples; and before and after etching of the Ge<sub>39</sub>Se<sub>61</sub> thin film. (Etching conditions: 10 mTorr, 700 W, 20 sccm and unbiased substrate holder)

In the Ge 2p<sub>3/2</sub> spectra of the Ge sample, the Ge-Ge bond is located at 1217.1 eV. Two additional peaks are needed to fit the Ge spectrum at 1217.6 eV (chemical shift, CS = 0.5 eV) and 1218.8 eV (CS = 1.9 eV). Based on the chemical shifts of these two components, the former describes the (Ge)<sub>3</sub>-Ge-F entity and the latter corresponds to the (Ge)-Ge-F<sub>3</sub> entity. Turning to the nonetched Ge-Se thin film, the dominant peak at 1218.8 eV is assigned to the [GeSe<sub>4/2</sub>] motif. The electronegativity of selenium (2.55) is higher than that of germanium (2.05), thus there is a chemical shift for that component to higher value (CS = 1.7 eV). As the sample remain untreated (no cleaning processes), the air exposure induces the Ge-O species located at 1219.5 eV (CS = 2.4 eV). In the spectrum of the etched Ge<sub>39</sub>Se<sub>61</sub> thin film, the dominant component (BE = 1218.8 eV), corresponds to the [GeSe<sub>4/2</sub>] motif. Since the analysis is performed after a 100% SF<sub>6</sub> etching process, surface is free of oxide, meaning that the contribution at 1220.1 eV (CS = 3.0 eV) is assigned to the (Se)-Ge-F<sub>3</sub> species. This attribution is supported by the energy shift of 1.5 eV starting from the [GeSe<sub>4/2</sub>] motif. At the surface (0 to 2.5

nm), Ge atoms have different chemical environments as compared to those within the near-surface layers (2.5 to 100 nm), resulting in Ge atoms bonded to 3 Se and 1 F; 2 Se and 2 F; 1 Se and 3 F *etc.*

Table 3: Fit values extracted from Ge 2p<sub>3/2</sub> and Ge 3d XPS spectra of nonetched Ge<sub>39</sub>Se<sub>61</sub> thin film; and after etching of Ge sample and Ge<sub>39</sub>Se<sub>61</sub> thin film at 10 mTorr, 700 W, 20 sccm and without bias. *BE: Binding Energy* ( $\pm 0.1$  eV); *FWHM: Full Width at Half Maximum* ( $\pm 0.05$  eV);  $\Delta E$ : *spin-orbit splitting* ( $\pm 0.05$  eV).

Sample	Entity	Ge 2p <sub>3/2</sub>			Ge 3d ( $\Delta E = 0.55$ eV)		
		BE (eV)	FWHM (eV)	Rel. Area	BE (eV)	FWHM (eV)	Rel. Area
Etched Ge	Ge-Ge	1217.1	1.04	100	29.0	0.55	100
	(Ge) <sub>3</sub> -Ge-F	1217.6	1.66	34.6	29.5	0.63	21.0
	(Ge)-Ge-F <sub>3</sub>	1218.9	1.58	20.7	30.8	0.45	1.6
Nonetched Ge-Se	GeSe <sub>4/2</sub>	1218.8	1.10	100	31.3	1.11	100
	Ge-O	1219.5	1.81	32.5	32.5	1.33	19.2
Etched Ge-Se	GeSe <sub>4/2</sub>	1218.8	1.54	100	31.3	1.11	100
	(Se)-Ge-F <sub>3</sub>	1220.1	1.84	19.0	33.1	1.53	4.8

Turning to the Ge 3d spectra, the doublets are related to those used for the decomposition of Ge 2p<sub>3/2</sub> spectra. One must consider that the inelastic mean free path of electrons is different according to the kinetic energy of the photoelectron. For an Al K $\alpha$  excitation, we calculate the inelastic mean free paths of Ge 2p<sub>3/2</sub> (kinetic energy,  $E_k \simeq 266$  eV) and Ge 3d ( $E_k \simeq 1456$  eV) photoelectrons at  $\sim 0.8$  nm and  $\sim 2.8$  nm, respectively [64]. However, the relative areas of the (Ge)<sub>3</sub>-Ge-F, (Ge)-Ge-F<sub>3</sub> and (Se)-Ge-F<sub>3</sub> doublets are lower here than in the Ge 2p<sub>3/2</sub> region (table 3). Considering the difference in inelastic mean free paths between Ge 2p<sub>3/2</sub> and Ge 3d, we interpret this result as a strong indication that the fluorinated products are mostly located in the first or second surface layers.

From 58 to 52 eV, the XPS spectra present the Se 3d contributions. The pure vitreous Se sample is decomposed with two doublets with primary components at 55.3 eV and 55.7 eV, respectively. These contributions originate from selenium rings and selenium chains [65,66]. No fluorinated species are clearly identified, even using a pure selenium sample. The exposure to reactive neutral species as F or SF<sub>x</sub> leads to a surface free of SeF<sub>x</sub> residues. At the surface of the nonetched Ge<sub>39</sub>Se<sub>61</sub> thin film, the doublet at 54.7 eV is attributed to the (Ge)-Se-Ge entity. The chemical shift between the Se-Se and the (Ge)-Se-Ge doublets (CS = - 0.6 eV) is also due to the difference of electronegativity between Se and Ge. A second doublet (BE = 55.3 eV) is needed to envelop the spectrum, ascribing the (Se)-Se-Ge entity. The decomposition of the etched Ge-Se thin film is carried out with one contribution at 54.7 eV assigned to the (Ge)-Se-Ge entity. It is also consistent with the fact that there is no Se-F bond after a 100% SF<sub>6</sub> etching process.

Table 4: Fit values extracted from Se 3p and Se 3d XPS spectra before and after etching of Se sample and Ge<sub>39</sub>Se<sub>61</sub> thin film at 10 mTorr, 700 W, 20 sccm and without bias. *BE*: Binding Energy ( $\pm 0.1$  eV); *FWHM*: Full Width at Half Maximum ( $\pm 0.05$  eV);  $\Delta E$ : spin-orbit splitting ( $\pm 0.05$  eV).

Sample	Entity	Se 3p ( $\Delta E = 5.75$ eV)			Se 3d ( $\Delta E = 0.85$ eV)		
		BE (eV)	FWHM (eV)	Rel. Area	BE (eV)	FWHM (eV)	Rel. Area
Nonetched Se	Se-Se	161.6	1.70	100	55.3	0.66	100
	Se-Se	162.1	2.28	22.1	55.7	0.72	22.1
Etched Se	Se-Se	161.6	1.81	100	55.3	0.80	100
	Se-Se	162.1	2.55	13.6	55.7	0.99	13.6
Nonetched Ge-Se	(Ge)-Se-Ge	161.0	1.87	100	54.7	0.84	100
	(Se)-Se-Ge	161.6	2.35	14.8	55.3	0.96	14.8
Etched Ge-Se	(Ge)-Se-Ge	161.0	2.07	100	54.7	1.18	100

The examples of Se 3p XPS spectra are presented in figure 6, and the extracted fit values are shown in table 4. Presence of sulphur is observed after etching on the Ge surface. The binding energy position at 162 eV is typical for elemental sulphur or Ge-S environment [67].

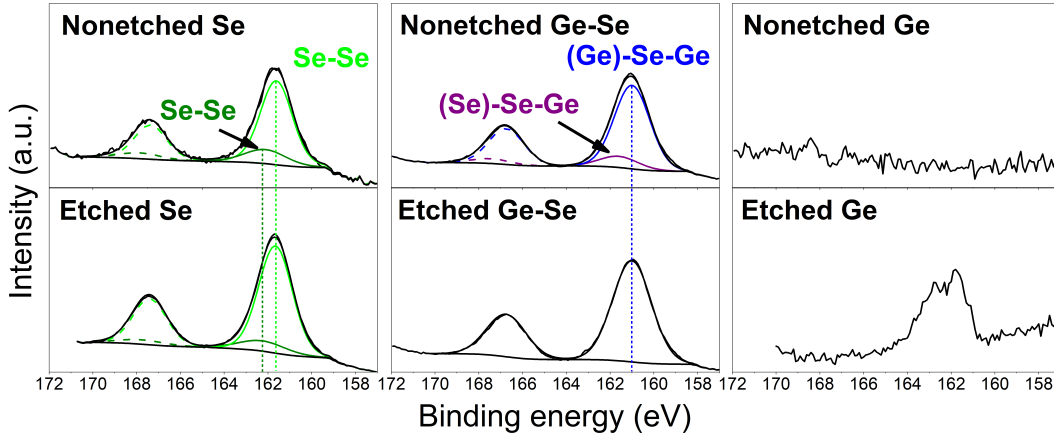


Figure 6: Se 3p XPS spectra before and after etching of Se (left); before and after etching of Ge<sub>39</sub>Se<sub>61</sub> thin film (middle); before and after etching of Ge (right). (*Etching conditions: 10 mTorr, 700 W, 20 sccm and unbiased substrate holder*)

Concerning the Se and Ge<sub>39</sub>Se<sub>61</sub> etched samples the overlap between the Se 3p and S 2p core levels makes the determination of the presence or absence of sulfur more difficult. Note that the kinetic energy of Se 3p photoelectrons ( $E_k \simeq 1325$  eV) is close to that of Se 3d photoelectrons ( $E_k \simeq 1431$  eV), and consequently, the chemical shifts and the relative areas of these core levels should be similar. These parameters are constrained with those of the Se 3d core level. Furthermore, a Se 3p<sub>3/2</sub>-Se 3p<sub>1/2</sub> ratio of 0.43 and a spin-orbit splitting of 5.75 eV are retrieved as fitting parameters using a Se nonetched

sample. These fit parameters were used for the decomposition of the Se 3p spectra of the Se and Ge<sub>39</sub>Se<sub>61</sub> etched samples. The congruence between the envelope spectra and the raw spectra indicates that sulfur atoms are most likely absent at the surface.

*3.1.4 Excited species* Figure 7 shows optical emission spectra recorded during the etching of the GeSe<sub>2</sub> glass target. Concerning Ge and Se, we assume that the emission lines result from the complete dissociation of volatile products followed by a direct or dissociative excitation (4a) and an electronic transition from an upper level A<sup>i</sup> to a lower level A<sup>j</sup> (4b). Photons may also originate from recombination processes between electrons and positive ions (4c).

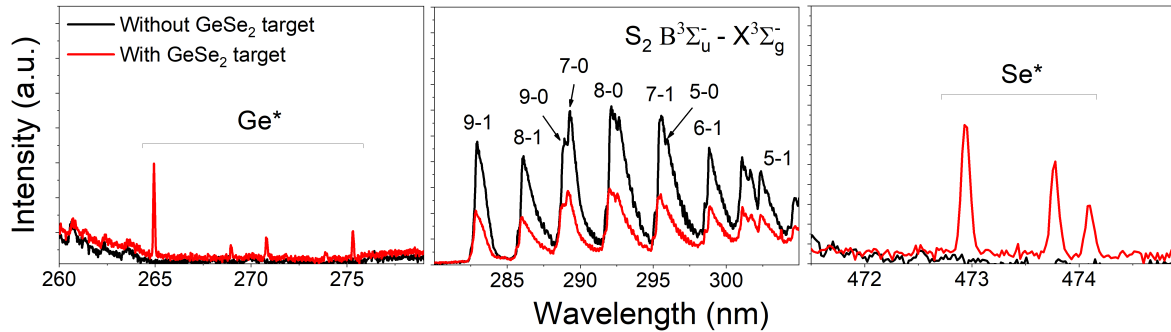
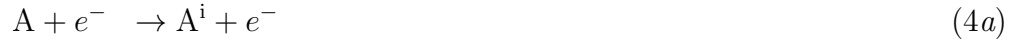
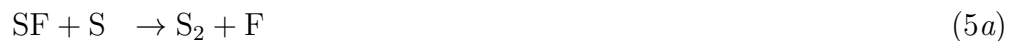


Figure 7: Optical emission spectra recorded without the GeSe<sub>2</sub> glass target (black line) and during the etching of the GeSe<sub>2</sub> glass target (red line) at 10 mTorr, 700 W, 20 sccm and without bias.

Ge emission lines result from the electronic transitions from the excited 4s<sup>2</sup>4p5s level to the ground 4s<sup>2</sup>4p<sup>2</sup> state. Both configurations contain a multitude of levels, leading to a rich Ge spectrum in the UV region [68]. However, the sensitivity of our measurements and the overlapping with the S<sub>2</sub> vibrational band [69] limit the identification to four lines. The reaction pathway leading to the S<sub>2</sub> molecules is mostly due to the SF reactive neutral recombination, leading to the S<sub>2</sub> (5a), S<sub>2</sub>F (5b) and SF<sub>2</sub> molecules, and their dissociation [70].



But, as the selenium is etched, the formation of SSeF<sub>x</sub><sup>+</sup> ions should consume the SF<sub>x</sub> reactive neutrals, explaining the drop of intensity for the S<sub>2</sub> band (figure 7). For

Se emission lines in the visible region of the spectrum, three lines are identified by comparing our spectrum with the work of Ruedy and Gibbs [71]. Unfortunately, there is no consistent literature about the GeF\* and SeF\* excited states. Nevertheless, it is expected that these unstable species are present inside the etching chamber since the formation of Ge\* and Se\* excited states arises from the dissociation of GeF<sub>x</sub> and SeF<sub>x</sub> species.

From MS and OES results, we propose simplified reaction schemes of fluorine-based etch products (figure 8).

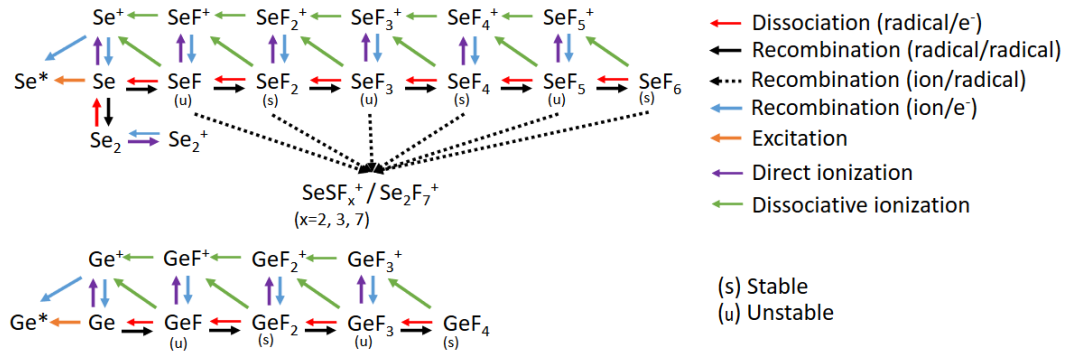


Figure 8: Reaction schemes for GeF<sub>x</sub> and Se<sub>x</sub>S<sub>y</sub>F<sub>z</sub> products.

### 3.2 Etching in SF<sub>6</sub>/Ar plasma

Figure 9 shows simulation data as the electronic density ( $n_e$ ), the electronic temperature ( $T_e$ ), the reactive neutral fluxes and the ion fluxes; along with the etch rate of the Ge<sub>39</sub>Se<sub>61</sub> thin films versus the argon percentage. Dominant species are plotted, excluding S, S<sup>+</sup>, SF, SF<sup>+</sup>, F<sub>2</sub> and F<sub>2</sub><sup>+</sup> species. Note that simulation data consider an Ar percentage of the total flow rate, whereas the etch rate measurements consider an Ar percentage of the total pressure. Nevertheless, similar trends of fluxes and plasma parameters are expected.

As a consequence of the large increase in the electron density (figure 9(a)), which increases excitation and dissociation events, argon addition produces only a slight decrease of the F atom flux (figure 9(b)). Concerning positive ions, Ar<sup>+</sup> is the dominant ion among all the ionic species in the 25-100% Ar range, moreover its flux increases typically in proportion to the Ar percentage in the mixture (figure 9(c)).

Experiments are carried out with an unbiased substrate holder, hence the positive ions strike the sample with a mean kinetic energy close to the plasma potential (< 10 eV). As such, sputtering by ion bombardment is inefficient because of the low sputtering yields [72]. As fluorine atoms do not compete with other species, the etch rate drops as the chemical contribution is removed from the etching process (figure 9(d)). A similar variation was observed on silica glasses [50] and tellurium-based chalcogenides [73], although the bias was set at - 200 V. Such results demonstrate the important role of surface chemistry reactions in the etching mechanisms.

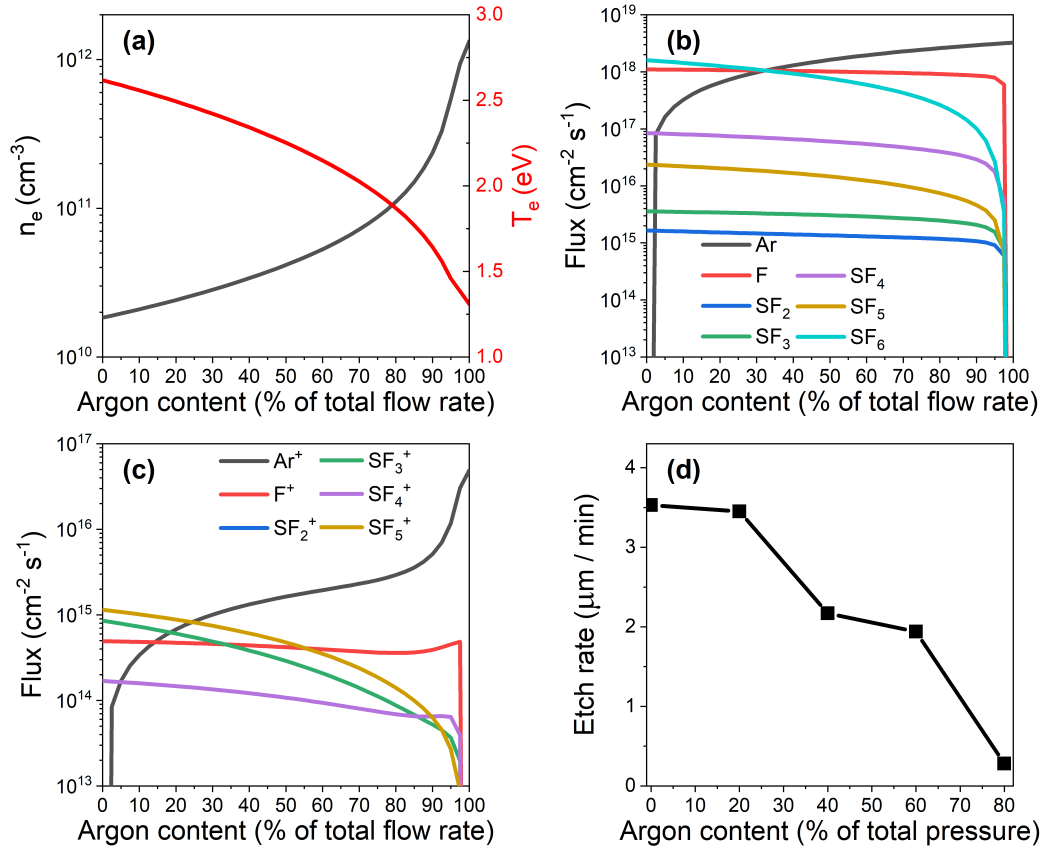


Figure 9: (a) Plasma parameters ( $n_e$ : electronic density;  $T_e$ : electronic temperature) (b) reactive neutral fluxes (c) positive ion fluxes according to argon percentage (% of total sccm) at 900 W, 10 mTorr and 40 sccm (modeling); and (d) etch rate of the Ge<sub>39</sub>Se<sub>61</sub> thin films according to argon percentage (% of total pressure) at 900 W, 10 mTorr and without bias.

As shown in figure 10, a variation of  $T_e$  has repercussion on the electron energy distribution. That is why each reaction should be regarded as probabilities which are mostly  $T_e$  dependent. As  $T_e$  decreases, the probabilities are less reduced for excitation mechanisms (Ge\*, Se\*) than those of dissociative ionization processes.

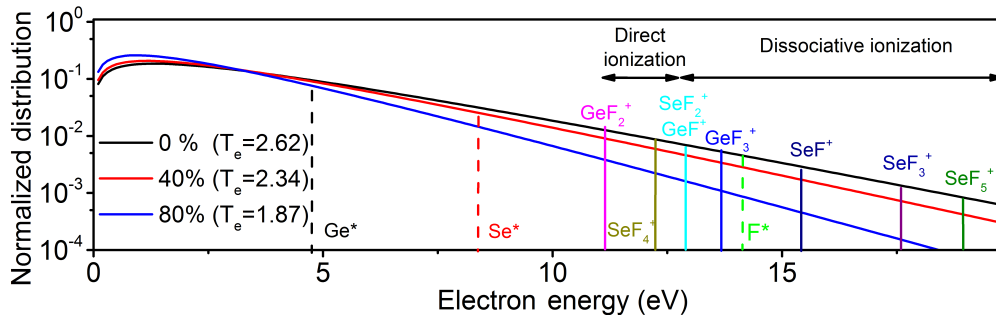


Figure 10: Maxwell-Boltzmann electron energy distribution as a function of  $T_e$ .

Evolution of the OES intensity data for selected emission lines with Ar content is shown in figure 11(a). In this experiment, actinometry cannot be carried out because of the modification of the plasma electrical parameters ( $n_e$  and  $T_e$ ) due to the high argon content. Nevertheless, from 100% SF<sub>6</sub> process to SF<sub>6</sub>/Ar (20%/80%), the Ge and Se emission line intensities increase slightly. This behaviour cannot be a consequence of a larger etch rate (figure 9(d)) and a larger density of Ge and Se etch products in the gas phase since both quantities drop when increasing the argon content in the mixture. The reason must therefore be sought within the plasma and to its characteristics that could lead to a higher dissociation of the Se and Ge etch products and excitation of Se and Ge atoms. Considering the variation of  $n_e$  and  $T_e$  estimated from the modeling (figure 9(a)) and the excitation energy threshold of the atoms from the ground state (table 1), it is likely that the increase of  $n_e$  contributes to the increase in intensity of Se and Ge emission.

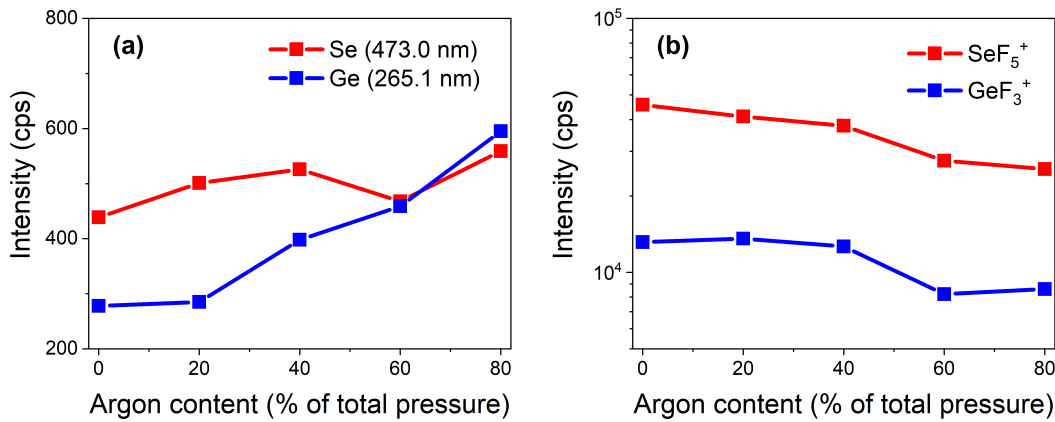


Figure 11: (a) OES and (b) MS data (reactive neutral analysis at an electron energy of 70 eV) during the etching of the GeSe<sub>2</sub> glass target as a function of argon percentage in the SF<sub>6</sub>/Ar mixture at 10 mTorr, 900 W and without bias.

Figure 11(b) presents MS data versus the Ar content. SeF<sub>6</sub> and GeF<sub>4</sub> reactive neutral products (detected as SeF<sub>5</sub><sup>+</sup> and GeF<sub>3</sub><sup>+</sup> ions) exhibit a variation similar to that of the fluorine atom flux, implying that the formation of SeF<sub>6</sub> and GeF<sub>4</sub> molecules is highly dependent on the fluorine concentration, although it cannot be fully correlated with the etch rate. Based on that result, we conclude that the production of SeF<sub>6</sub> and GeF<sub>4</sub> should not be exclusively assimilated to desorption processes.

### 3.3 Etching in SF<sub>6</sub>/O<sub>2</sub> plasma

It is known that adding oxygen to a fluorine precursor increases the fluorine atomic density by reducing the recombination time of the precursor fragments. The O<sub>2</sub> fragments interact with SF<sub>x</sub> reactive neutral species and recombine into SO<sub>x</sub>F<sub>y</sub> molecules [74–76].

Direct evidences of oxidation are shown in figure 12 by means of *in situ* XPS where Ge, Se and  $Ge_{39}Se_{61}$  samples are etched simultaneously. In the case of the  $Ge_{39}Se_{61}$  thin films, an insulating surface is formed because of the oxide layer. The latter generates a charging effect, which shifts the original spectra to higher values of binding energy. Based on the previous observation in Sec. 3.1.3, it is believed that the (Ge)-Se-Ge environment (BE = 54.7 eV) remains at the surface, regardless of the etching condition. Thus, it is taken as the reference value for the calibration of  $Ge_{39}Se_{61}$  XPS spectra.

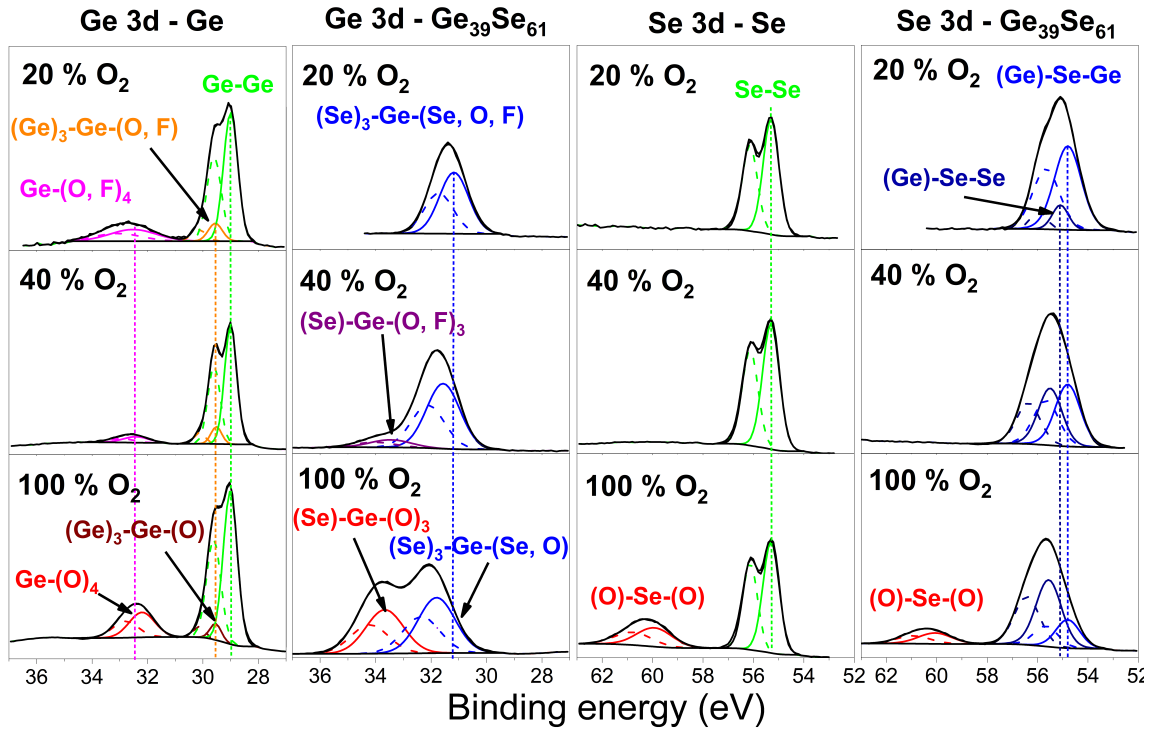


Figure 12: Ge 3d and Se 3d XPS spectra after the etching of the Ge and Se samples; and the  $Ge_{39}Se_{61}$  thin films as a function of oxygen content in the  $SF_6/O_2$  mixture. (Etching conditions: 10 mTorr, 900 W and unbiased substrate holder)

The decomposed Ge 3d spectra for the Ge sample exhibit the  $Ge-(O, F)_4$  species (CS = 3.5 eV), which arise from oxygen and fluorine adsorption on the surface. The doublet becomes fluorine-depleted as the oxygen percentage increases in the  $SF_6/O_2$  mixture, and so, the doublet shifts to a lower value of binding energy, ascribing the  $Ge-(O)_4$  species (CS = 3.3 eV) at 100% of  $O_2$ . The first oxidation and fluorinated states is represented by the  $(Ge)_3-Ge-(O, F)$  environment at 29.6 eV (CS = 0.6 eV) and the  $(Ge)_3-Ge-(O)$  environment at 29.5 eV (CS = 0.5 eV). After the etching of the  $Ge_{39}Se_{61}$  thin films, it is believed that the additional adsorption of fluorine and oxygen generates the nonvolatile  $GeSe_xO_yF_z$  species. The  $(Se)_3-Ge-(Se, O, F)$  doublet envelops the  $GeSe_{4/2}$  motif and the  $(Se)_3-Ge-(O, F)$  environments. The doublet is located at 31.2 eV (CS = 2.2 eV) at 20% of  $O_2$ , and it shifts to 31.6 eV (CS = 2.6 eV) at 40% of  $O_2$ . In a 100%  $O_2$  etching process, the doublet is fluorine-depleted, leading to the

(Se)<sub>3</sub>-Ge-(Se, O) environments (BE = 31.8 eV). The etching process also generates the (Se)-Ge-(O, F)<sub>3</sub> and (Se)-Ge-(O)<sub>3</sub> positioned at 33.5 eV (CS = 4.5 eV) and 33.6 eV (CS = 4.6 eV), respectively. Oxidation is obvious with the relative areas of these doublets in comparison to those of (Se)<sub>3</sub>-Ge related doublets.

Turning to the Se 3d spectra, whether it is for the Se or Ge<sub>39</sub>Se<sub>61</sub> sample, there are no (O, F)-Se-(O, F) environments at 20 or 40% of oxygen. Nevertheless, the etching generates the (Ge)-Se-Se environment which shifts progressively to higher values of binding energy with the increasing O<sub>2</sub> content. At the surface, the formation of Ge-O bonds and the absence of Se-O bonds are likely to rearrange the chemical environment of Se atoms. After a 100% O<sub>2</sub> etching process, the O-Se-O environment is detected at 59.9 eV (CS = 4.6 eV) for the Se sample and 60.1 eV (CS = 4.8 eV) for the Ge-Se thin film.

Area ratios calculated from XPS spectra are presented in table 5. Oxidation of the surface is evidenced by the increasing (Se)-Ge-R<sub>3</sub>/(Se)<sub>3</sub>-Ge-R and (O)-Se-(O)/(Ge, Se)-Se-Ge area ratios with the O<sub>2</sub> percentage in the SF<sub>6</sub>/O<sub>2</sub> mixture. In addition, according to the inelastic mean free path calculation, 95% of the Ge 2p<sub>3/2</sub> and Ge 3d photoelectrons describe the Ge neighbouring atoms within 2.47 and 8.40 nm of the depth of analysis, respectively. The decrease of the area ratio with the kinetic energy (*e.g.* from Ge 2p<sub>3/2</sub> to Ge 3d) is interpreted as an oxygen depletion along the depth of analysis. The low proportion of Se-O bonds suggests that oxygen likely has a higher affinity for germanium than for selenium.

In presence of a high concentration of oxygen, oxides are formed by oxygen adsorption. GeO, GeO<sub>2</sub>, SeO<sub>2</sub> and SeO<sub>3</sub> respectively have a boiling point at 710°C, 1115°C, 118°C and 350°C. Furthermore, Ge-O bond (657.5 ± 4.6 kJ/mol) requires more energy than Ge-Se (484.7 ± 1.7 kJ/mol), Se-Se (330.5 kJ/mol) and Ge-Ge (264.4 ± 6.8 kJ/mol) bonds to break [77]. Therefore, formation of oxides at the surface slows down the etch rate (table 5).

Table 5: Etch rate of Ge<sub>39</sub>Se<sub>61</sub> thin films and area ratios extracted from Ge<sub>39</sub>Se<sub>61</sub> XPS spectra (figure 12). (*R* = *O*, *F*, *Se*)

% of O <sub>2</sub> in SF <sub>6</sub> /O <sub>2</sub> (of total pressure)	Etch rate (μm/min)	Area ratio		
		(Ge 2p <sub>3/2</sub> ) $\frac{(\text{Se})-\text{Ge}-\text{R}_3}{(\text{Se})_3-\text{Ge}-\text{R}}$	(Ge 3d) $\frac{(\text{Se})-\text{Ge}-\text{R}_3}{(\text{Se})_3-\text{Ge}-\text{R}}$	(Se 3d) $\frac{(\text{O})-\text{Se}-(\text{O})}{(\text{Ge,Se})-\text{Se}-\text{Ge}}$
0	3.53		n/a	
10	3.79		n/a	
20	3.63	0	0	0
30	2.09		n/a	
40	1.31	0.7	0.14	0
100	n/a	3.2	1.3	0.15

Contrary to the SF<sub>6</sub>/Ar plasma, actinometry is valid in SF<sub>6</sub>/O<sub>2</sub> plasma because of

low Ar content (2% of the total pressure) regarding those of SF<sub>6</sub> and O<sub>2</sub> [46]. Despite the data do not reveal specific values of the F and O atom densities, actinometry describes their variation as a function of the O<sub>2</sub> content. In figure 13(a), the F/Ar intensity ratio has a maximum at 30% of O<sub>2</sub>. Such variation of the F/Ar ratio is a direct consequence of the conversion of the SF<sub>6</sub> into other gases (SO<sub>x</sub>F<sub>y</sub>, F<sub>2</sub>, *etc.*). Similar curves of the F/Ar intensity ratio have been obtained, or can be retrieved in extensive amount of studies related to fluorine-based plasmas [45,74,78]. Simultaneously, for an O<sub>2</sub> percentage lower than 10%, the oxygen atom density is believed to be negligible because of recombination processes leading to SO<sub>x</sub>F<sub>y</sub> molecules.

In this experiment, the maximum of etch rate (3.79 μm/min) is found at 10% of O<sub>2</sub>, and the etch rate cannot be correlated with the F/Ar intensity ratio as displayed in figure 13(a). As demonstrated with *in situ* XPS analysis, fluorine and oxygen atoms compete for the active sites on the Ge<sub>39</sub>Se<sub>61</sub> surface. Nevertheless, the fraction of active sites occupied increases with the density of oxygen atoms whose variation is represented by the O/Ar intensity ratio. The etch rate is sharply reduced when the oxygen coverage is too significant because of the formation of the (Se)-Ge-R<sub>3</sub> related doublets (R = O, F) at the surface, regardless of the fluorine atomic density.

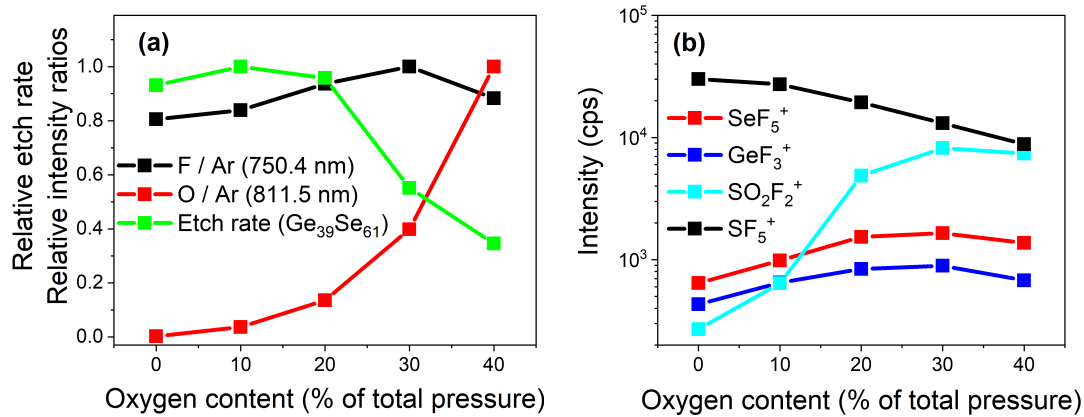


Figure 13: (a) Normalized etch rate and normalized intensity ratios (OES) and (b) MS data (reactive neutral analysis at an electron energy of 70 eV) during the etching of the GeSe<sub>2</sub> glass target as a function of the oxygen content in the SF<sub>6</sub>/O<sub>2</sub> mixture at 10 mTorr, 900 W and without bias.

The recombination reactions are observable by means of mass spectrometry measurements (figure 13(b)), by monitoring the SO<sub>2</sub>F<sub>2</sub><sup>+</sup> ion (m/z 102) which presents also a maximum at 30% of O<sub>2</sub>. GeF<sub>3</sub><sup>+</sup> and SeF<sub>5</sub><sup>+</sup> ions, formed inside the mass spectrometer source, also present a similar variation. These MS signals are correlated with the F/Ar intensity ratio but not with the etch rate, confirming that other processes than the desorption of GeF<sub>4</sub> and SeF<sub>6</sub> are involved in the production of GeF<sub>4</sub> and SeF<sub>6</sub>. For an O<sub>2</sub> percentage greater than about 30%, the decrease of ion signals is attributed to the decrease of the fluorine atomic density. The conversion of SeF<sub>6</sub> to SeO<sub>x</sub>F<sub>y</sub> is highly probable. However, the large number of products (SO<sub>x</sub>F<sub>y</sub>, GeF<sub>x</sub> and SeF<sub>x</sub>) limits the

interpretation because of the overlapping on the range mass of SeO<sub>2</sub>F<sup>+</sup> (m/z 128 to 136) and SeO<sub>2</sub>F<sub>2</sub><sup>+</sup> (m/z 147 to 155).

#### 4 Conclusion

Etching mechanisms of the Ge<sub>39</sub>Se<sub>61</sub> thin films and the GeSe<sub>2</sub> chalcogenide glass were investigated combining plasma and surface diagnostics in Inductively Coupled Plasmas. The identification of etch products was crucial to, thereafter, monitor some of them as a function of plasma conditions. That is why, the etch products were identified during the etching of a GeSe<sub>2</sub> glass target in a 100% SF<sub>6</sub> plasma. Using the appearance potentials, we classified SeF<sub>*x*</sub> (*x* = 2, 4, 6) and GeF<sub>*x*</sub> (*x* = 2, 4) as stable and volatile species, and we noticed a strong analogy between SeF<sub>*x*</sub> and SF<sub>6</sub> fragmentation spectra. Simultaneously to MS analysis, we compared OES spectra with and without the presence of a GeSe<sub>2</sub> glass target to identify Ge and Se emission lines in the UV and visible regions (200 to 500 nm).

*In situ* XPS study showed contributions of GeF<sub>*x*</sub> species at the surface, although the latter was negligible compared to the Ge-Se chemical state in the Ge 3d region. The results indicated that fluorine-based products are mostly located in the first layer at the surface. It can be speculated that GeF<sub>2</sub> molecule originates from the gas phase reactions within the plasma and not from desorption mechanisms. SeF<sub>*x*</sub> species were not noticed, implying that SeF<sub>*x*</sub> are desorbed at the substrate working temperature. In addition, sulfur contribution remained undetected at the surface of Se-containing materials, but a small contribution was found at the surface of Ge etched sample. Overall, XPS showed a relatively small amount of fluorine-based products, confirming that fluorine is an efficient etching agent for the Ge-Se materials.

The study of ionic products proved that SF<sub>*x*</sub> species play a role during the etching of Se-containing materials because of the formation of SeSF<sub>*x*</sub><sup>+</sup> ions. These species result from ion-molecule reactions with SF<sub>*x*</sub> radicals. Since such reactions were noticed with O and S elements resulting in S<sub>*x*</sub>O<sub>*y*</sub>F<sub>*z*</sub> etch products, further studies should be focused on ion-molecule reactions during the etching of Te-based materials to confirm if there are shared properties between all chalcogen elements. Another analogy between selenium and sulfur fluorine-based products was found with the presence of Se<sub>2</sub>F<sub>7</sub><sup>+</sup> and the absence of Se<sub>2</sub>F<sub>*x*</sub><sup>+</sup> (*x* = 1-6).

The case of the SF<sub>6</sub>/O<sub>2</sub> mixture showed that oxidation of the surface, more specifically the formation of Ge-O bonds, results in the decrease of the etch rate and product signals on mass spectrometry measurements.

In conclusion, the etching of Ge-Se materials in SF<sub>6</sub> plasma offers some advantages due to the chemical etching contribution. It is believed that GeF<sub>*x*</sub><sup>-</sup> and SeF<sub>*x*</sub><sup>-</sup> are also produced during the etching process, therefore mass spectrometry analysis should be extended for the identification of negative ions to provide a complete overview of the plasma chemistry. The understanding of etching mechanisms could be improved by investigating the etching on patterned thin films.

## Acknowledgments

Czech Science Foundation (project no. 19-24516S) and the Barrande exchange program between France and the Czech Republic are greatly acknowledged for supporting this work.

## References

- [1] Petit L, Carlie N, Chen H, Gaylord S, Massera J, Boudebs G, Hu J, Agarwal A, Kimerling L and Richardson K 2009 *J. Solid State Chem.* **182** 2756–2761
- [2] Choi J W, Han Z, Sohn B U, Chen G F R, Smith C, Kimerling L C, Richardson K A, Agarwal A M and Tan D T H 2016 *Sci. Rep.* **6** 1–8
- [3] Abdellaoui N, Starecki F, Boussard-Plédel C, Shpotyuk Y, Doualan J L, Braud A, Baudet E, Němec P, Chevire F, Dussauze M, Bureau B, Camy P and Nazabal V 2018 *Opt. Mater. Express* **8** 2887
- [4] Starecki F, Braud A, Abdellaoui N, Doualan J L, Boussard-Plédel C, Bureau B, Camy P and Nazabal V 2018 *Opt. Express* **26** 26462–26469
- [5] Su X, Wang R, Luther-Davies B and Wang L 2013 *Appl. Phys. A* **113** 575–581
- [6] Olivier M, Němec P, Boudebs G, Boidin R, Focsa C and Nazabal V 2015 *Opt. Mater. Express* **5** 781–793
- [7] Eggleton B J, Luther-Davies B and Richardson K 2011 *Nat. Photonics* **5** 141–148
- [8] Adam J L and Zhang X 2014 *Chalcogenide Glasses: Preparation, Properties and Applications* (Woodhead Publishing)
- [9] González-Leal J M, Ledesma A, Bernal-Oliva A M, Prieto-Alcón R, Márquez E, Angel J A and Cárabe J 1999 *Mater. Lett.* **39** 232–239
- [10] Jarvis R A, Wang R P, Rode A V, Zha C and Luther-Davies B 2007 *J. Non-Cryst. Solids* **353** 947–949
- [11] Baudet E, Sergent M, Němec P, Cardinaud C, Rinnert E, Michel K, Jouany L, Bureau B and Nazabal V 2017 *Sci. Rep.* **7** 3500
- [12] Verger F, Nazabal V, Colas F, Němec P, Cardinaud C, Baudet E, Chahal R, Rinnert E, Boukerma K, Peron I, Deputier S, Guilloux-Viry M, Guin J P, Lhermite H, Moreac A, Compère C and Bureau B 2013 *Opt. Mater. Express* **3** 2112–2131
- [13] Němec P, Jedelský J, Frumar M, Štábl M, Černošek Z and Vlček M 2004 *Philos. Mag.* **84** 877–885
- [14] Baudet E, Cardinaud C, Boidin R, Girard A, Gutwirth J, Němec P and Nazabal V 2018 *J. Am. Ceram. Soc.* **101** 3347–3356
- [15] Madden S J, Choi D Y, Bulla D A, Rode A V, Luther-Davies B, Ta'eed V G, Pelusi M D and Eggleton B J 2007 *Opt. Express* **15** 14414–14421
- [16] Yoon S M, Lee N Y, Ryu S O, Park Y S, Lee S Y, Choi K J and Yu B G 2005 *Jpn. J. Appl. Phys.* **44** L869
- [17] Baudet E, Gutierrez-Arroyo A, Němec P, Bodiou L, Lemaitre J, Sagazan O D, Lhermitte H, Rinnert E, Michel K, Bureau B, Charrier J and Nazabal V 2016 *Opt. Mater. Express* **6** 2616–2627
- [18] Hu J, Tarasov V, Agarwal A, Kimerling L, Carlie N, Petit L and Richardson K 2007 *Opt. Express* **15** 2307–2314
- [19] Choi D Y, Madden S, Rode A, Wang R and Luther-Davies B 2007 *Appl. Phys. Lett.* **91** 011115
- [20] Charrier J, Anne M L, Lhermite H, Nazabal V, Guin J P, Charpentier F, Jouan T, Henrio F, Bosc D and Adam J 2008 *J. Appl. Phys.* **104** 073110
- [21] Bodiou L, Starecki F, Lemaitre J, Nazabal V, Doualan J L, Baudet E, Chahal R, Gutierrez-Arroyo A, Dumeige Y, Hardy I, Braud A, Soulard R, Camy P, Němec P, Palma G, Prudenzeno F and Charrier J 2018 *Opt. Mater.* **75** 109–115
- [22] Molnar B J and Dove D B 1974 *J. Non-Cryst. Solids* **16** 149–160

- [23] Matsuda O, Inoue K and Murase K 1990 *Solid State Commun.* **75** 303–308
- [24] Petri I, Salmon P S and Fischer H E 2000 *Phys. Rev. Lett.* **84** 2413–2416
- [25] Kumar R T A, Lekha P C, Sundarakannan B and Padiyan D P 2012 *Philos. Mag.* **92** 1422–1434
- [26] Bureau B, Troles J, Le Floch M, Guénot P, Smektala F and Lucas J 2003 *J. Non-Cryst. Solids* **319** 145–153
- [27] Edwards T, Sen S and Gjersing E 2012 *J. Non-Cryst. Solids* **358** 609–614
- [28] Micoulaut M, Kachmar A, Bauchy M, Le Roux S, Massobrio C and Boero M 2013 *Phys. Rev. B* **88** 054203
- [29] Olivier M, Tchahame J C, Němec P, Chauvet M, Besse V, Cassagne C, Boudebs G, Renversez G, Boidin R, Baudet E and Nazabal V 2014 *Opt. Mater. Express* **4** 525–540
- [30] Zha C, Wang R, Smith A, Prasad A, Jarvis R A and Luther-Davies B 2007 *J Mater Sci: Mater Electron* **18** 389–392
- [31] Němec P, Zhang S, Nazabal V, Fedus K, Boudebs G, Moreac A, Cathelinaud M and Zhang X H 2010 *Opt. Express* **18** 22944–22957
- [32] Němec P, Frumarová B and Frumar M 2000 *J. Non-Cryst. Solids* **270** 137–146
- [33] Mao A W, Aitken B G, Youngman R E, Kaseman D C and Sen S 2013 *J. Phys. Chem. B.* **117** 16594–16601
- [34] Oehrlein G S, Bestwick T D, Jones P L, Jaso M A and Lindström J L 1991 *J. Electrochem. Soc.* **138** 1443
- [35] Campo A, Cardinaud C and Turban G 1995 *J. Vac. Sci. Technol. B. Microelectron. Nanometer Struct.* **13** 235–241
- [36] Wongwanitwattana C, Shah V A, Myronov M, Parker E H C, Whall T and Leadley D R 2014 *J. Vac. Sci. Technol. A* **32** 031302
- [37] Ahles C F, Choi J Y, Wolf S and Kummel A C 2017 *ACS Appl Mater Interfaces* **9** 20947–20954
- [38] Kim T S, Yang H Y, Kil Y H, Jeong T S, Kang S and Shim K H 2009 *J. Korean Phys. Soc.* **54** 2290–2296
- [39] Shim K H, Kil Y H, Yang H D, Park B K, Yang J H, Kang S, Jeong T S and Kim T S 2012 *Mater. Sci. Semicond. Process.* **15** 364–370
- [40] Darnon M, de Lafontaine M, Volatier M, Fafard S, Arès R, Jaouad A and Aimez V 2015 *J. Vac. Sci. Technol. B* **33** 060605
- [41] Idris A S, Jiang H and Hamamoto K 2016 *Electron. Lett.* **52** 1868–1869
- [42] Chen W R, Chang S J, Su Y K, Lan W H, Lin A C H and Chang H 2000 *Jpn. J. Appl. Phys.* **39** 3308
- [43] Pearton S J and Ren F 1993 *J. Vac. Sci. Technol. B* **11** 15–19
- [44] Eddy C R, Leonhardt D, Shamamian V A and Butler J E 2001 *J. Electron. Mater.* **30** 538–542
- [45] Coburn J W and Chen M 1980 *J. Appl. Phys.* **51** 3134–3136
- [46] Lopaev D V, Volynets A V, Zyryanov S M, Zotovich A I and Rakhimov A T 2017 *J. Phys. D: Appl. Phys.* **50** 075202
- [47] Kramida A, Yu Ralchenko, Reader J and and NIST ASD Team 2019 NIST Atomic Spectra Database (ver. 5.7.1), [Online]. Available: <https://physics.nist.gov/asd> [2017, April 9]. National Institute of Standards and Technology, Gaithersburg, MD.
- [48] Shirley D A 1972 *Phys. Rev. B* **5** 4709–4714
- [49] Lallement L, Rhallabi A, Cardinaud C, Peignon-Fernandez M C and Alves L L 2009 *Plasma Sources Sci. Technol.* **18** 025001
- [50] Lallement L, Gosse C, Cardinaud C, Peignon-Fernandez M C and Rhallabi A 2010 *J. Vac. Sci. Technol. A* **28** 277–286
- [51] Pateau A, Rhallabi A, Fernandez M C, Boufnichel M and Roqueta F 2013 *J. Vac. Sci. Technol. A* **32** 021303
- [52] Chantry P J 1987 *J. Appl. Phys.* **62** 1141–1148
- [53] Ryan K R and Plumb I C 1990 *Plasma Chem. Plasma Process.* **10** 207–229
- [54] Lee C and Lieberman M A 1995 *J. Vac. Sci. Technol. A* **13** 368–380

- [55] Tarnovsky V, Deutsch H, Martus K E and Becker K 1998 *J. Chem. Phys.* **109** 6596–6600
- [56] Christophorou L G and Olthoff J K 2000 *J. Phys. Chem. Ref. Data* **29** 267–330
- [57] Rauf S, Ventzek P L G, Abraham I C, Hebner G A and Woodworth J R 2002 *J. Appl. Phys.* **92** 6998–7007
- [58] *TRCVP Vapor Pressure Database Version 2.2P* (Thermodynamic Research Center Texas A&M University College Station TX)
- [59] Dibeler V H and Molher F 1948 *J. Res. Natl. Bur. Stand.* **40** 25–29
- [60] Harland P W, Cradock S and Thynne J C J 1972 *Int. J. Mass Spectrom.* **10** 169–195
- [61] Picard A, Turban G and Grolleau B 1986 *J. Phys. D: Appl. Phys.* **19** 991
- [62] Rumble J 2017 *CRC Handbook of Chemistry and Physics, 98th Edition* 98th ed (Boca Raton London New York: Taylor & Francis Ltd.)
- [63] Sauers I and Harman G 1992 *J. Phys. D: Appl. Phys.* **25** 761–773
- [64] Powell C J and Jablonski A 2010 *NIST Electron Inelastic-Mean-Free-Path Database - Version 1.2* (National Institute of Standards and Technology, Gaithersburg, MD)
- [65] Hohl D, Jones R O, Car R and Parrinello M 1987 *Chem. Phys. Lett* **139** 540–545
- [66] Goldan A H, Li C, Pennycook S J, Schneider J, Blom A and Zhao W 2016 *J. Appl. Phys.* **120** 135101
- [67] Chen H, Keiser C, Du S, Gao H J, Sutter P and Sutter E 2017 *Phys. Chem. Chem. Phys.* **19** 32473–32480
- [68] L Andrew K and W Meissner K W 1959 *J. Opt. Soc. Am.* **49** 146–159
- [69] Sadeghi N, Debontride H, Turban G and Peignon M C 1990 *Plasma Chem. Plasma Process.* **10** 553–569
- [70] Brunning J and Clyne M A A 1984 *J. Chem. Soc., Faraday Trans. 2* **80** 1001–1014
- [71] Ruedy J E and Gibbs R C 1934 *Phys. Rev.* **46** 880–888
- [72] Behrisch R and Eckstein W (eds) 2010 *Sputtering by Particle Bombardment: Experiments and Computer Calculations from Threshold to MeV Energies* softcover reprint of hardcover 1st ed. 2007 edition ed (Berlin; New York: Springer)
- [73] Zhang Z, Song S, Song Z, Cheng Y, Zhu M, Li X, Zhu Y, Guo X, Yin W, Wu L, Liu B, Feng S and Zhou D 2014 *Appl. Surf. Sci.* **311** 68–73
- [74] d’Agostino R, Cramarossa F, Benedictis S D, Fracassi F, Láska L and Mašek K 1985 *Plasma. Chem. Plasma. Process.* **5** 239–253
- [75] Ryan K R 1989 *Plasma Chem. Plasma Process.* **9** 483–496
- [76] Snijkers R J M M, Coulon J F and Turban G 1991 *J. Phys. D: Appl. Phys.* **24** 1098–1101
- [77] Luo Y R 2007 *Comprehensive Handbook of Chemical Bond Energies* (CRC Press)
- [78] Morshed M M and Daniels S M 2012 *Plasma Sci. Technol.* **14** 316